Predictive Filtering in Motion Compensation with Steerable Cardiac Catheters

Paul M. Loschak, Alperen Degirmenci, and Robert D. Howe

***Abstract*— Robotic cardiac catheterization using ultrasound (US) imaging catheters provides real time imaging from within the heart while reducing the difficulty in manually steering a four degree-of-freedom (4-DOF) catheter. Accurate robotic catheter navigation in the heart is challenging due to a variety of disturbances including cyclical physiological motions, such as respiration. In this work we compensate for respiratory motion by using an Extended Kalman Filter (EKF) to predict target motion and by applying the predictions to steer the US imaging catheter. The system performance was measured in bench top experiments with phantom vasculature. The robotic system with predictive filtering tracked cyclically moving targets with 1.59 mm and 0.72° mean error. Accurately tracking moving structures can improve intra-procedural treatments and visualization.**

I. Introduction

A number of cardiac interventional and diagnostic tasks can be performed minimally invasively using cardiac catheters [1]. Automated steering of cardiac ultrasound (US) imaging catheters, which feature an US transducer in the distal catheter tip, can potentially enhance imaging of cardiac structures and working instruments. Accurate automated catheter steering in the heart is difficult due to many disturbances, including those from cyclical physiological motions such as heart beat and respiration. Predictive filtering and motion compensation applied to catheter steering can enable continuous US imaging of or interaction with targets (Fig. 1). Automated techniques may improve clinical outcomes, save time, and ease mental and physical burdens on clinicians.

Commercially available robotic catheter systems offer solutions for teleoperation, enabling clinicians to manipulate a catheter at a safe distance from X-ray fluoroscopy radiation exposure during intra-procedural visualization [2]–[6]. Research prototypes have demonstrated automated steering with cardiac catheters [7]–[12] and endoscope-size manipulators [13] in constrained bench top environments. Motion tracking work on frequency-based models has not yet been applied to motion compensation [14], [15], or has focused on rigid robotic tools only [16], [17]. A limited number of flexible manipulator research prototypes have demonstrated motion compensation through *in vivo* animal testing: 1D cardiac motion compensation with a non-steerable cardiac guidewire [18] and 3D respiratory motion compensation with a steerable endoscope [19].

This work was supported by the Harvard University John A. Paulson School of Engineering and Applied Sciences, American Heart Association Grant #15PRE22710043, the National Institutes of Health Grant #1R21EB018938, and the NVIDIA Academic Hardware Grant Program.

All authors are with the John A. Paulson School of Engineering and Applied Sciences, Harvard University, Cambridge, MA 02138 USA. R.D. Howe is also with the Harvard - MIT Division of Health Sciences & Technology, Cambridge, MA 02139 USA. E-mail: {loschak, adegirmenci, howe}@seas.harvard.edu.

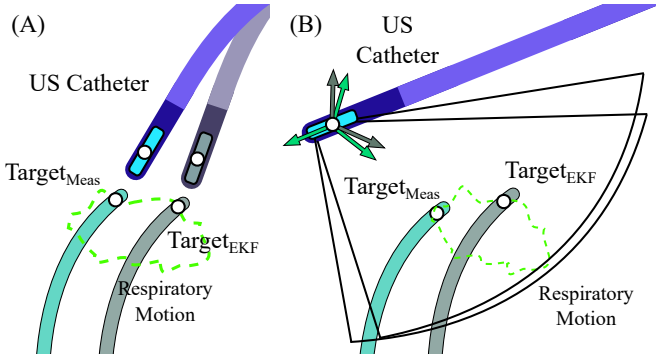

Fig. 1. Predictive filtering is applied towards the measured target position, Target$_{Meas}$, in two types of instrument tracking. (*A*) In position-based instrument tracking the tip of the ultrasound (US) catheter is navigated towards the predicted target position, Target$_{EKF}$. (*B*) In imager-based instrument tracking the tip of the US catheter is fixed in place while the US imager is rotated to point towards the predicted target position, Target$_{EKF}$.

Automated cardiac catheter steering prototypes have not yet been shown to navigate accurately *in vivo* or with motion compensation. We have begun to address the difficulties of steering cardiac catheters *in vivo* in our development of a system for automatically pointing cardiac imaging catheters in constrained bench top settings [20] and by rejecting disturbances to the catheter body during *in vivo* animal experiments [21]. In this work we focus on a predictive filter for steering cardiac catheters to perform cyclical target tracking at respiratory speeds in bench top experiments. The following sections describe the motivation for cyclical target tracking, methods for predictive filtering, bench top experiments, and results. This paper presents the first work known to the authors on steering cardiac catheters using predictive filtering.

II. Background

A. Ultrasound Catheters

While the motion compensation methods presented in this work are generally applicable to flexible manipulators, this investigation focuses on US catheters for cardiac procedures. Catheters are long, thin, flexible composite plastic tubes controlled from outside the patient at the proximal end. US catheters feature a transducer in the distal tip to acquire US images of instruments and tissue structures inside the patient. The distal tip, typically inserted into the vasculature via the groin, can be guided to the internal chambers of the heart or into other organ systems. US catheters are

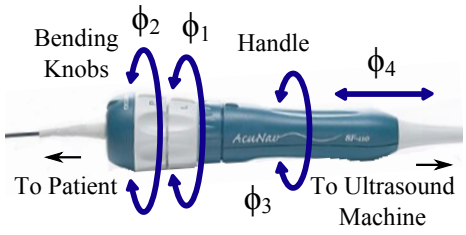

Fig. 2. AcuNav US imaging catheter handle showing control DOFs.

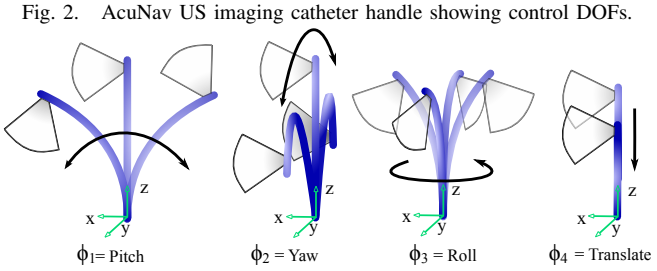

Fig. 3. Joint inputs and corresponding tip motions adjust the US imaging plane.

useful because they can provide high resolution views during cardiac procedures, but manually pointing the imager at a target requires extensive training and skill.

The US catheter is manually manipulated by grasping the catheter handle and actuating each of the four degrees of freedom (4-DOF), as in Fig. 2, to create the tip adjustments shown in Fig. 3. The catheter handle can be rotated or translated (inserted/retracted). Four pull wires spaced apart $90°$ along the cross-section of the catheter shaft connect the distal end of the catheter to two handle knobs. The two bending knobs connect to pairs of opposing pull wires. The distal end bending section is constructed from softer materials compared to the rest of the catheter shaft. As a result, pull wire actuation causes significant bending at the 5 cm distal bending section and moderate bending through the rest of shaft. The most distal 2 cm section of the tip contains the US transducer (64-element 2D US). AcuNav is currently the most widely used intracardiac US catheter (AcuNav, Biosense Webster, Diamond Bar, CA, USA). The 8 Fr size catheter (diameter 2.67 mm) with length 90 cm was used to validate the system in our studies.

B. Unconstrained Catheter Motion

Our initial work on 4-DOF catheter steering relied on a set of physical constraints which isolated bending to only the distal 5 cm bending section of the tip [20]. The bending section base was fixed with respect to the rest of the catheter and robot. These constraints were relaxed in later work towards *in vivo* experiments, and a new control strategy was developed to be robust against disturbances to the catheter body [21].

C. Respiratory Motion

We now combine robust control for unconstrained catheter motion with predictive filtering for catheter-based target tracking. During cardiac procedures the US catheter experiences cyclical physiological disturbances from respiration and heartbeat. Cyclical disturbances affect each region of the

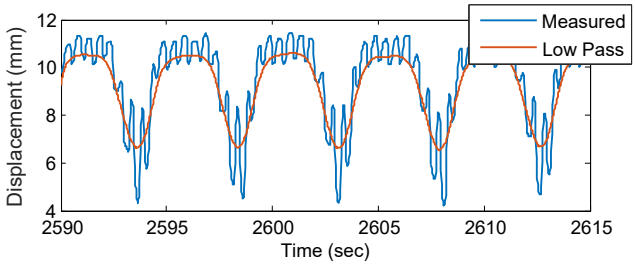

Fig. 4. Pre-recorded *in vivo* catheter tip displacement data used for developing the predictive filter.

heart differently, and the US imager can become misaligned with the target it is imaging. A method for tracking and compensating for cyclical motions is therefore needed.

The AcuNav catheter materials were designed for dozens of manual bending cycles, thereby making heartbeat motion compensation impractical beyond short periods of time with the currently used off-the-shelf US catheters. Fast catheter motions are also difficult to achieve when manipulating the catheter handle, as opposed to manipulating the pull wires directly (as in some commercial prototypes [6]). We can, however, demonstrate lower-frequency respiratory motion compensation with existing off-the-shelf AcuNav catheters. We do this while building a framework which can compensate for cyclical motions at cardiac frequencies (assuming the robot hardware and communications are sufficiently high bandwidth as well).

Pre-recorded catheter tip displacement data from *in vivo* porcine tests were used to analyze respiratory motions and develop the predictive filter. An US catheter was outfitted with electromagnetic (EM) trackers (6-DOF trakSTAR, Ascension Technology/NDI, Ontario, Canada) and introduced to the right heart. The system measured catheter pose disturbance from breathing and heartbeat motion. The US catheter handle was not actuated during measurements.

The raw data demonstrated pose changes resulting from both cardiac ($2\ Hz$) and respiratory ($0.2\ Hz$) motions. The data were zero-phase low pass filtered to eliminate cardiac motion (low pass filter order 50, Hamming window, cut off frequency $2\ Hz$). An example is shown in Fig. 4, where the blue line represents measured data (heartbeat and respiration) and the red line represents low pass filtered (respiration only). The low pass filtered data were truncated on either side due to the edge effects. The pre-recorded respiratory data were then used to develop the tracking algorithm.

III. Methods

Fig. 1 demonstrates two types of tracking. Fig. 1(A) shows position-based target tracking: the tip of the catheter is navigated to meet the position of the target. This will be demonstrated at respiratory speeds due to current off-the-shelf catheter limitations. This method will be applicable to cardiac motion compensation in later studies. Fig. 1(B) shows imager-based target tracking: the US catheter tip is steered to maintain the same position while rotating the US imager to synchronize with the target. This is directly

applicable to automatically steering US catheters for continuous target visualization. We develop this framework for motion compensation with cardiac catheters by examining physiological motions, representing respiratory motion with a frequency-based model, and developing a predictive filtering method.

A. Modeling Respiratory Disturbance

We zero-phase low pass filter the raw cyclical disturbances (Fig. 4) and then define periodic models for the isolated respiratory motion. Each coordinate of the tip position (x, y, z) is modeled separately. The in-depth calculations are available in [17], which was an expansion of [22]. Abbreviated calculations are given here for completeness.

We approximate the 1D signal, $y(t)$, with a limited number of harmonics, m. This is represented as an m-order time-varying Fourier series with a constant offset,

$$y\left(t\right) = c\left(t\right) + \sum_{i=1}^{m} r_i\left(t\right) \sin\theta_i\left(t\right), \tag{1}$$

where $\theta_i\left(t\right) = i\int_0^t \omega\left(\tau\right) d\tau + \phi_i\left(t\right)$. Here c is the constant offset, r_i and ϕ_i are the harmonic amplitudes and phases, $i \in (1, \ldots, m)$, and ω is the respiratory rate. The state vector model can be defined as

$$\boldsymbol{x}\left(t\right) \triangleq \begin{bmatrix} c(t) \\ r_i(t) \\ \omega(t) \\ \theta_i(t) \end{bmatrix}. \tag{2}$$

This model is initialized by measuring motion for at least two breaths ($> 10\ sec$). The initialization data collected are $\tilde{\boldsymbol{z}} \triangleq [z(0), z(\Delta t), \ldots, z((N-1)\Delta t)]^T$, where N refers to the total number of initialization points and Δt is the time between measurement acquisitions (mean sampling rate $\Delta t = 0.0234\ sec$ for the EM tracking system used). The harmonic amplitudes and coefficients are then obtained using a nonlinear least squares estimation. The state estimate at the moment of initialization is $\hat{\boldsymbol{x}}[k|k]$. We employ a discrete time notation where the current time step is $t = k$. In this notation convention, $\hat{\boldsymbol{x}}[k + M_1|k - M_2]$ is the state estimate at $t + M_1\Delta t$ based on information from $t - M_2\Delta t$.

This initialization strategy is done for each of the three axes, generating individual state representation models of movement in the x-, y-, and z-axes. Models were evaluated with $m = 4$ because additional harmonics had minimal impact on decreasing error at the cost of increased computational costs. An example model is shown in Fig. 5. The blue line represents the raw EM measurements of the y-axis. The black line represents the low pass filtered y-axis with the edge effects removed. The red line represents the initialized Fourier series model estimate. The mean absolute error between the y-axis model values and the low pass filtered measurements was $0.057\ mm$ ($\sigma = 0.041\ mm$). Not shown in the figure, the mean absolute model error for the x-axis was $0.037\ mm$ ($\sigma = 0.027\ mm$) and for the z-axis was $0.039\ mm$ ($\sigma = 0.028\ mm$).

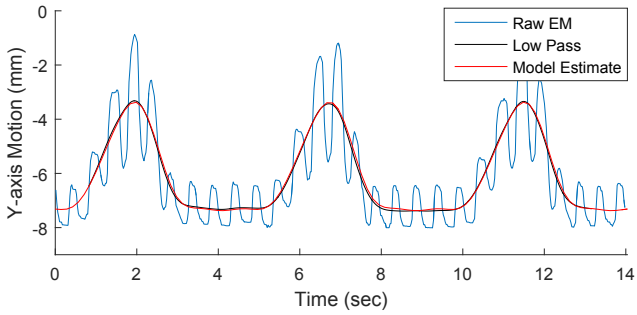

Fig. 5. Breathing model of low pass filtered y-coordinate motion.

B. Predicting Target Motion

Compensation for cyclical motions requires continuously measuring the target position and updating the controller setpoints accordingly. Multiple time delays in the system cause the catheter motion to lag behind the target, resulting in poor target tracking. Therefore a multi-step Extended Kalman Filter (EKF) was designed to continuously estimate the future target position and adjust the US catheter steering ahead of time (Fig. 6). The multi-step EKF uses outdated information (due to the low pass filter window edge effect) to estimate the target position farther into the future (due to hardware/software limitations).

Each coordinate of the target position (x, y, z) is filtered separately. The signal model in (2), $\boldsymbol{x}(t)$, is the state at a given point in time. The prediction calculations are as follows. We assume the Fourier components evolve through a random walk. The state space model for the system is

$$\hat{\boldsymbol{x}}\left[k + M_1\right] = \boldsymbol{F_M}\left[k\right]\hat{\boldsymbol{x}}\left[k - M_2\right] + \boldsymbol{\mu}[k], \tag{3}$$

where $\boldsymbol{F_M}\left[k\right]$ is the prediction matrix

$$\boldsymbol{F_M}\left[k\right] = \begin{bmatrix} \boldsymbol{I}_{m+1} & & \boldsymbol{0} & & \\ & 1 & & & \\ & M\Delta t & 1 & & \\ \boldsymbol{0} & 2M\Delta t & & 1 & \\ & \vdots & & & \ddots \\ & mM\Delta t & & & 1 \end{bmatrix} \tag{4}$$

and $\boldsymbol{\mu}[k]$ is the random step of the states. The random steps are assumed to be drawn from a zero mean multivariate

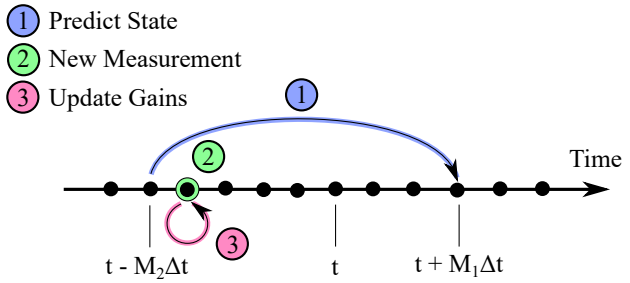

Fig. 6. Multi-step EKF uses past reliable information to predict a future time step. New measurements are used to update the Kalman gains for the past.

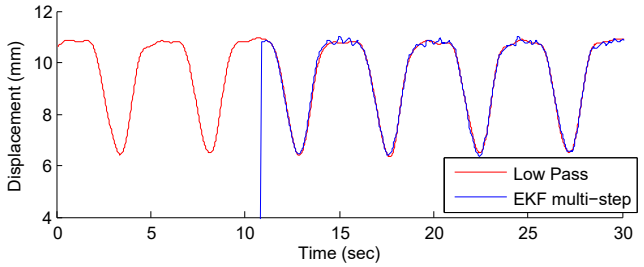

Fig. 7. Low pass filtered CT displacement and multi-step EKF simulation from pre-recorded data.

normal distribution represented by the environment uncertainty covariance matrix, $\boldsymbol{Q}$. The total number of samples to predict, M, is defined as $M = M_1 + M_2$. The EKF predicts ahead M_1 samples due to hardware and software limitations. M_2 refers to the most recently acquired samples which are not usable after low pass filtering due to the windowing edge effect.

The second part to the model is

$$z\left[k - M_2\right] = h\left(\hat{\boldsymbol{x}}\left[k - M_2\right]\right) + \nu\left[k - M_2\right]. \quad (5)$$

Here $z\left[k - M_2\right]$ is the latest usable measurement of the signal, $h\left(\hat{\boldsymbol{x}}\left[k - M_2\right]\right)$ is defined as $y\left[k - M_2\right]$, and $\nu\left[k - M_2\right]$ is zero mean Gaussian measurement noise with variance σ_R^2.

With this model we estimate the $2m+2$ model parameters of $\boldsymbol{x}$. The EKF estimates the nonlinear problem by linearizing about the current state estimate, $\hat{\boldsymbol{x}}[k - M_2|k - M_2]$. The prediction for the state $\hat{\boldsymbol{x}}\left[k + M_1\right]$ is calculated using (3). Then (1) is used to calculate the predicted value of the signal, $y\left[k + M_1\right]$. Next we use the current covariance matrix $\boldsymbol{P}\left[k - M_2\right]$ to predict the covariance matrix $\boldsymbol{P}\left[k + M_1\right]$ as in

$$\boldsymbol{P}[k+M_1|k-M_2] = \boldsymbol{F_M}\boldsymbol{P}[k-M_2|k-M_2]\boldsymbol{F_M}^T + \boldsymbol{Q}. \quad (6)$$

The Kalman gain, $\boldsymbol{K}\left[k + M_1\right]$, is calculated by

$$\boldsymbol{K}[k + M_1] = \boldsymbol{P}[k + M_1|k - M_2]\boldsymbol{H}[k + M_1]^T S^{-1} \quad (7)$$

$$S = \sigma_R^2 + \boldsymbol{H}[k + M_1]\boldsymbol{P}[k + M_1|k - M_2]\boldsymbol{H}[k + M_1]^T$$

and the sensor matrix $\boldsymbol{H}\left[k + M_1\right]$ is defined by (8).

After predictions for the state, the covariance matrix, and the Kalman gain are made, the system calculates the estimated target position and then calculates control commands to navigate the robot. Control commands are given to the robot actuators while the system waits for the next sensor measurement. As the next measurement becomes available, the recent measurements are low pass filtered. The most recent usable low pass filtered measurement is $z\left[k - M_2 + 1\right]$ (which represents time $t - (M_2 + 1)\Delta t$). This new measurement is then compared with the predicted value in order to update the state estimate, $\hat{\boldsymbol{x}}\left[k - M_2 + 1|k - M_2 + 1\right]$, and the covariance matrix, $\boldsymbol{P}\left[k - M_2 + 1|k - M_2 + 1\right]$, as in (9)-(10).

The covariance matrix, $\boldsymbol{P}$, is initialized as (11) where σ_R^2 is the measurement noise variance, σ_1^2 is the uncertainty of the amplitude components, σ_ω^2 is the uncertainty of the fundamental frequency, and σ_θ^2 is the uncertainty of the phase components. Trial and error by [22] determined that $\sigma_\theta^2 = 0.02\ rad^2$. The environment uncertainty covariance matrix, $\boldsymbol{Q}$, is a diagonal matrix with all values set to 10^{-4} except for q_ω.

1) Predictive Filter Simulation: The EKF was tested on pre-recorded data from early *in vivo* animal trials. The low pass filter edge effect parameter was set to $M_2 = 35$ samples ($0.819\ sec$). Predictions were calculated for the future time point at $M_1 = 20$ steps ($0.468\ sec$, experimentally determined). The first N data points were used for initializing the breathing model and calculating the first state, covariance matrix, and Kalman gain. Data points were then given to the EKF sequentially to simulate the sensors measuring live.

The EKF predicted the state for the future time point. Then the next measurement was given to the EKF and the multi-step EKF cycle repeated until the end of the data set. Fig. 7 shows the results of the simulation. The red line represents the low pass filtered tip displacement. The blue line, which begins at $t \approx 12\ sec$ after initialization, represents each predicted signal point based on only pre-existing information. The mean absolute error between each predicted value and the measured value was $0.088\ mm$ ($\sigma = 0.114\ mm$).

IV. Control Strategy

The US catheter is accurately navigated by combining predictive filtering, instrument tracking calculations, disturbance rejection inverse kinematics [21], and robot control [23] as in Fig. 8. Cyclical target movement (zero-phase low pass filtered to isolate respiratory motion) is modeled and predicted by the multi-step EKF (Fig. 8 green box). The pre-kinematics calculations then use the predicted target location, $X_{Target,Pred}$, along with user-defined control mode to calculate the required US catheter tip space adjustments, ΔX (Fig. 8 yellow box). The ΔX are calculated to either steer the catheter tip position to meet the target (position-based tracking) or rotate the US imager to point towards the target (imager-based tracking). The robust disturbance rejection inverse kinematics of [21] are then used to calculate the required joint space adjustments, $\Delta\Phi$. The joint space adjustments are scaled ($K < 1$) and input to the joint PID controllers (Fig. 8 orange box). The US catheter handle is adjusted and the catheter tip is navigated accordingly. This cycle repeats as the US catheter and target are measured by sensors. The EKF continuously updates the respiratory motion model to adapt to slight variations over time, improving prediction accuracy.

V. Experiments and Results

A. Experimental Setup

The bench top testing setup is shown in Fig. 9. The robot was designed to actuate the 4-DOF US catheter handle [23]. The catheter was manually introduced through the introducer and guided through the plastic IVC tube towards the motion simulator. The motion simulator is a plastic fixture that was designed to cyclically move the tracking target (an EM sensor) at respiratory amplitudes and frequencies.

$$\boldsymbol{H}[k+M_1]^T \triangleq \left(\frac{\partial h}{\partial x}\right)^T\Bigg|_{\hat{\boldsymbol{x}}[k+M_1|k-M_2]=\boldsymbol{F_M}\hat{\boldsymbol{x}}[k-M_2|k-M_2]} = \begin{bmatrix} 1 \\ \sin\theta_1[k+M_1|k-M_2] \\ \vdots \\ \sin\theta_m[k+M_1|k-M_2] \\ 0 \\ r_1[k+M_1|k-M_2]\cos\theta_1[k+M_1|k-M_2] \\ \vdots \\ r_m[k+M_1|k-M_2]\cos\theta_m[k+M_1|k-M_2] \end{bmatrix} \tag{8}$$

$$\hat{\boldsymbol{x}}\left[k-M_2+1|k-M_2+1\right] = \boldsymbol{F_M}\hat{\boldsymbol{x}}[k-M_2|k-M_2] + \boldsymbol{K}[k-M_2+1]\left(z[k-M_2+1] - h\left[\boldsymbol{F_M}\hat{\boldsymbol{x}}[k-M_2|k-M_2]\right]\right) \tag{9}$$

$$\boldsymbol{P}\left[k-M_2+1|k-M_2+1\right] = (\boldsymbol{I} - \boldsymbol{K}[k-M_2+1]\boldsymbol{H}[k-M_2+1])\boldsymbol{P}[k-M_2+1|k-M_2] \tag{10}$$

$$\boldsymbol{P}[k|k] = diag\left[\frac{\sigma_R^2}{N} \quad \sigma_1^2 \quad \frac{\sigma_1^2}{2^2} \quad \dots \quad \frac{\sigma_1^2}{m^2} \quad \sigma_\omega^2 \quad \sigma_\theta^2 \quad \dots \quad \sigma_\theta^2\right] \tag{11}$$

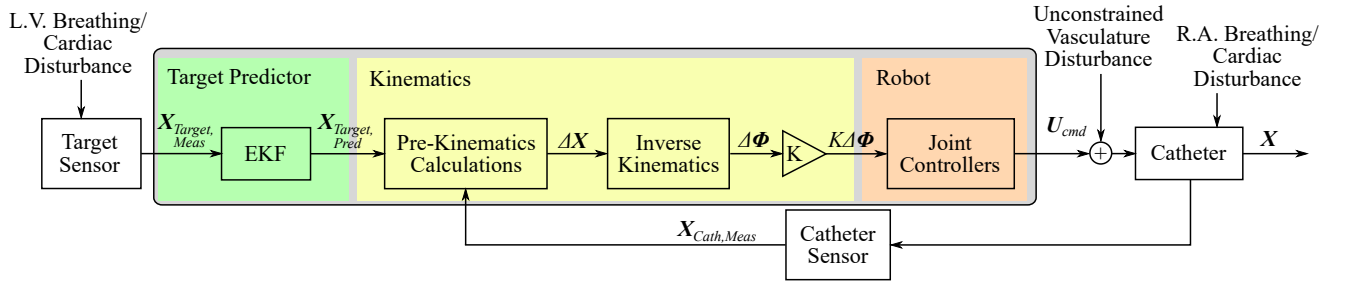

Fig. 8. Control diagram for instrument tracking with predictive filtering. (L.V. = left ventricle, R.A. = right atrium)

The EM tracking system has RMS accuracy $1.4\ mm$ and $0.5°$ and resolution $0.5\ mm$ and $0.1°$. The bench top setting was designed for low magnetic interference. Each robot DOF was actuated by a brushless DC motor and digital positioning controllers (Maxon Motors, Switzerland) running internal servo loops at $1\ kHz$.

B. Target Tracking: Position Mode

Target tracking tests were done with and without the EKF in order to demonstrate the benefits of predictive filtering in cyclical physiological motion compensation. The target was attached to the respiratory motion simulator with period $5\ sec$ and amplitude $\approx 13\ mm$. The US catheter was first made to follow the target without the EKF. The controller reacted to the measured target motion and adjusted the tip accordingly. Eleven tests were conducted for a combined total $268\ sec$ of tracking. An example data set is shown in Fig. 10(*top*). The desired x-axis is plotted in blue and the measured tip x-coordinate is plotted in red.

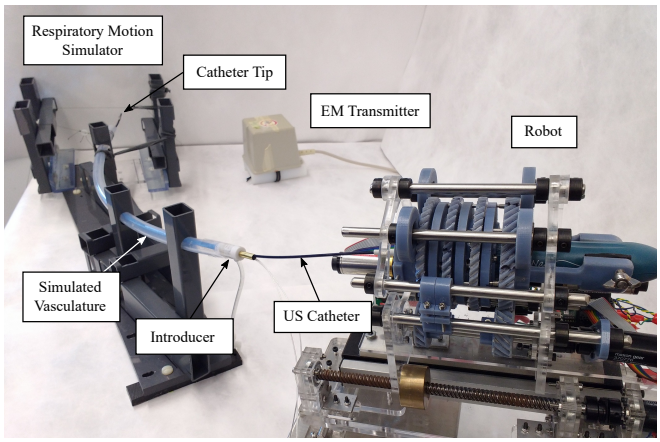

Fig. 9. Bench top experimental setup.

A similar set of tracking tests was done with the EKF enabled. Thirteen tests were conducted for 742 seconds of tracking. An example data set is shown in Fig. 10(*middle*). Fig. 10 (*bottom*) compares the total errors between non-EKF and EKF tests.

Experimental results are reported in Table I. First, the mean absolute errors across all tracking tests were calculated for non-EKF and EKF cases. The total percentage of time the system maintained the US catheter tip positioning error within $1\ mm$ and $2\ mm$ was reported for both cases in Table I and in Fig. 11. Without the EKF enabled, the catheter tip continuously followed the target except for the moments when the target changed direction and the catheter lagged behind it. The position error peaked during each direction change of the target. The mean of the peak errors and the mean time delay before catching up to the target were measured for both non-EKF and EKF cases.

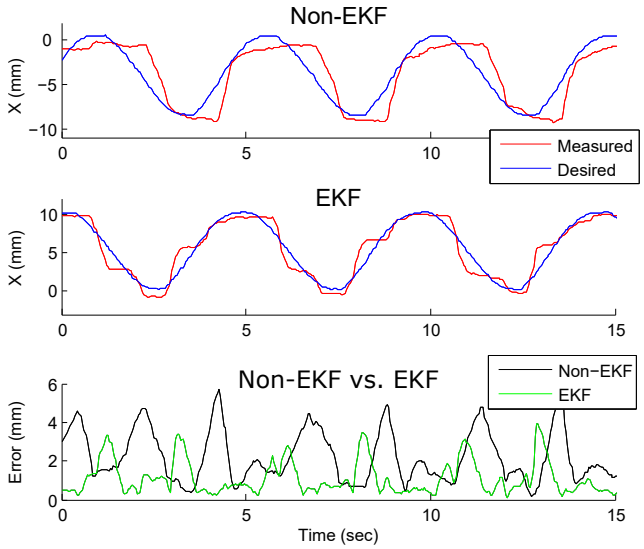

Fig. 10. Position tracking a cyclically moving target: (*top*) Controller tracking error without predictive filtering (non-EKF). (*middle*) Controller tracking error with predictive filtering (EKF). (*bottom*) Compare tracking error without EKF (black) and with EKF (green).

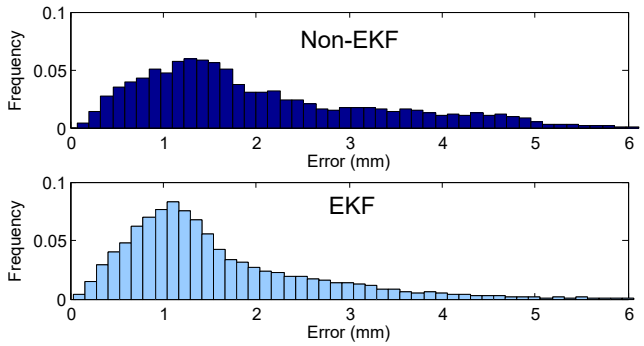

Fig. 11. Resulting percentage of samples within a certain error range, with and without EKF.

TABLE I

INSTRUMENT TRACKING POSITION RESULTS.

Metric	Without EKF: Mean (σ)	With EKF: Mean (σ)
Position error (mm)	2.00 (1.25)	1.59 (1.10)
Time within 1 mm (%)	22.16	31.80
Time within 2 mm (%)	60.97	75.24
Peak error (mm)	4.64 (0.76)	3.68 (0.94)
Time delay (sec)	0.63 (0.12)	0.29 (0.25)

C. Target Tracking: Imager Mode

The target was attached to the respiratory motion simulator with period 5 sec and amplitude $\approx$ 16 mm. The system continuously rotated the US imager to align with the target while the tip of the catheter was made to stay at the same position. The angle between the imager and the target ranged from 0° to 3°, 5°, or 8° for different tests. The results between tests were similar. Twenty tests without the EKF were done for a combined total 510 seconds. An example data set, Fig. 12 (*top*), shows the error angle between the US imager and the target.

A similar set of tests was done with the EKF enabled.

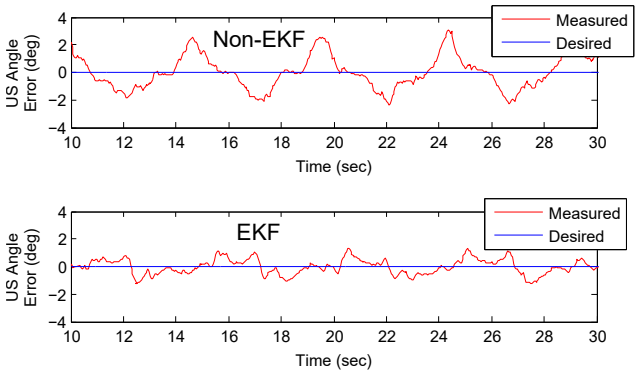

Fig. 12. Pointing the US imager at a cyclically moving target: (*top*) Controller tracking error without predictive filtering (non-EKF). (*middle*) Controller tracking error with predictive filtering (EKF).

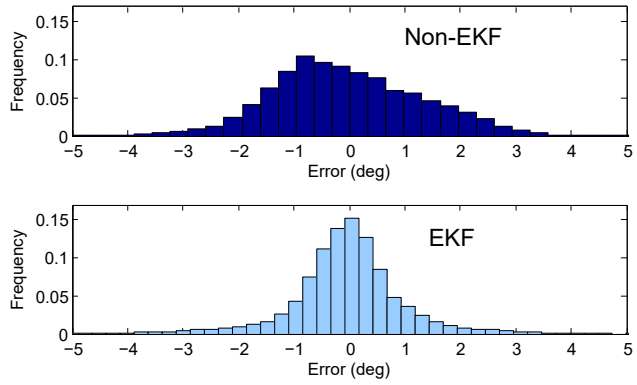

Fig. 13. Resulting percentage of samples within a certain error range, with and without EKF.

TABLE II

INSTRUMENT TRACKING IMAGER RESULTS.

Metric	Without EKF: Mean (σ)	With EKF: Mean (σ)
Angle error (°)	1.15 (1.27)	0.72 (0.78)
Position error (mm)	0.50 (0.37)	0.46 (0.32)
Time within 0.5° (%)	26.89	52.07
Time within 1° (%)	52.92	77.93
Time within 2° (%)	85.65	92.86
Time within 1 mm (%)	90.09	91.34
Time within 2 mm (%)	99.56	99.91
Peak error (°)	2.39 (0.74)	2.01 (1.04)
Time delay (sec)	0.68 (0.40)	0.34 (0.24)

Twenty individual tests were done for a combined total 631 seconds. An example data set is shown in Fig. 12 (*bottom*). The results in Table II report many of the same performance metrics as well as additional metrics regarding US imager alignment. Mean overall errors are reported for both tip position and alignment angle. The percentages of time the US imager was aligned with the target within 0.5°, 1°, and 2° were reported in Table II and Fig. 13.

VI. DISCUSSION

The system successfully applied the multi-step EKF towards steering a cardiac catheter to compensate for cyclical target motions. Two modes were demonstrated: position and imager tracking. The position tracking method was

successfully demonstrated at respiratory speeds (not cardiac speeds due to current off-the-shelf catheter material constraints). This is also applicable towards compensating for higher frequency cardiac motions. The imager tracking mode demonstrated the clinically relevant task of automatically re-orienting the US imager towards a target moving at respiratory speeds.

Bench top experimental target tracking results were reported by several metrics of tracking quality. Position tracking mode results demonstrated improvement by EKF in all categories. Position errors on the order of 1-2 mm during position-based tracking are sufficient for performing a wide range of procedures. Imager tracking mode results demonstrated improvement by EKF in categories related to angular adjustment. Imager alignment angle errors on the order of 1-2° and position errors of 1 mm during imager-based tracking are sufficient for imaging working instruments and cardiac anatomy. Imager tracking mode results related to positional adjustments were approximately equal between non-EKF and EKF tests.

While predictive filtering experiments demonstrated improvement, some tracking error still persisted. For example, Fig. 10(*top*) showed tracking errors in the x-axis resulting from a combination of system lag and pull wire mechanics after direction changes. In Fig. 10(*middle*) the lag was mitigated by the predictive filter and the remaining error was from pull wire mechanics. The y- and z-axes exhibited similar behavior. Future work aims to manage pull wire mechanics and further reduce tracking errors.

EKF prediction accuracy may be improved by examining other cardiac frequency filtering techniques to reduce M_2 and modifying the robot design to reduce M_1. Additionally, position mode target tracking at cardiac speeds can be achieved by designing custom-built steerable catheters which are robust to thousands of bending cycles. Future developments in imager-based tracking will move towards *in vivo* studies by compensating for cyclical respiratory motion disturbances to the catheter while also using predictive filtering to track a moving target.

VII. Conclusions

A predictive filtering algorithm was applied towards target tracking with cardiac catheters. A framework for compensating for cyclical physiological motions was presented. Bench top experiments demonstrated two types of motion compensation and tracking at respiratory speeds. The system aims to improve diagnosis and treatments with cardiac catheters by automatically providing enhanced intra-procedural US visualizations of cardiac structures and working instruments.

ACKNOWLEDGMENT

The authors would like to acknowledge Laura J. Brattain, PhD, Yaroslav Tenzer, PhD, James Weaver, PhD, Cory M. Tschabrunn, and Elad Anter, MD.

References

[1] M. Moscucci, *Grossman & Baim's Cardiac Catheterization, Angiography, and Intervention*. Lippincott Williams & Wilkins, 2013.

[2] I. Corindus. (2016) Corindus, Inc. *CorPath Robotic PCI*. [Online]. Available: http://www.corindus.com/

[3] I. Catheter Robotics. (2016) Catheter Robotics, Inc. *Amigo Remote Catheter System*. [Online]. Available: http://www.catheterrobotics.com/

[4] Stereotaxis. (2016) Stereotaxis *V-Drive Robotic Navigation System*. [Online]. Available: http://www.stereotaxis.com/products/vdrive/

[5] I. Stereotaxis. (2016) Stereotaxis *Niobe ES*. [Online]. Available: http://www.stereotaxis.com/products/niobe/

[6] I. Hansen Medical. (2016) Hansen Medical, Inc. *Sensei X Robotic Catheter System*. [Online]. Available: http://hansenmedical.com

[7] R. S. Penning, J. Jung, J. A. Borgstadt, N. J. Ferrier, and M. R. Zinn, "Towards closed loop control of a continuum robotic manipulator for medical applications," in *Robotics and Automation (ICRA), 2011 IEEE International Conference on*. IEEE, 2011, pp. 4822–4827.

[8] R. J. Webster and B. A. Jones, "Design and kinematic modeling of constant curvature continuum robots: A review," *The International Journal of Robotics Research*, 2010.

[9] M. Khoshnam, M. Azizian, and R. V. Patel, "Modeling of a steerable catheter based on beam theory," in *Robotics and Automation (ICRA), 2012 IEEE International Conference on*. IEEE, 2012, pp. 4681–4686.

[10] Y. Ganji and F. Janabi-Sharifi, "Catheter kinematics for intracardiac navigation," *Biomedical Engineering, IEEE Transactions on*, vol. 56, no. 3, pp. 621–632, 2009.

[11] D. B. Camarillo, C. R. Carlson, and J. K. Salisbury, "Configuration tracking for continuum manipulators with coupled tendon drive," *Robotics, IEEE Trans. on*, vol. 25, no. 4, pp. 798–808, 2009.

[12] M. C. Yip and D. B. Camarillo, "Model-less hybrid position/force control: a minimalist approach for continuum manipulators in unknown, constrained environments," *IEEE Robotics and Automation Letters*, vol. 1, no. 2, pp. 844–851, 2016.

[13] G. J. Vrooijink, T. Ellenbroek, P. Breedveld, J. G. Grandjean, and S. Misra, "A preliminary study on using a robotically-actuated delivery sheath (rads) for transapical aortic valve implantation," in *Robotics and Automation (ICRA), 2014 IEEE International Conference on*. IEEE, 2014, pp. 4380–4386.

[14] C. Riviere, A. Thakral, I. Iordachita, G. Mitroi, and D. Stoianovici, "Predicting respiratory motion for active canceling during percutaneous needle insertion," in *Engineering in Medicine and Biology Society, 2001. Proceedings of the 23rd Annual International Conference of the IEEE*, vol. 4. IEEE, 2001, pp. 3477–3480.

[15] A. Thakral, J. Wallace, D. Tomlin, N. Seth, and N. V. Thakor, "Surgical motion adaptive robotic technology (smart): Taking the motion out of physiological motion," in *International Conference on Medical Image Computing and Computer-Assisted Intervention*. Springer, 2001, pp. 317–325.

[16] C. N. Riviere, R. S. Rader, and N. V. Thakor, "Adaptive cancelling of physiological tremor for improved precision in microsurgery," *IEEE Transactions on Biomedical Engineering*, vol. 45, no. 7, pp. 839–846, 1998.

[17] S. G. Yuen, D. T. Kettler, P. M. Novotny, R. D. Plowes, and R. D. Howe, "Robotic motion compensation for beating heart intracardiac surgery," *The International Journal of Robotics Research*, vol. 28, no. 10, pp. 1355–1372, 2009.

[18] S. B. Kesner and R. D. Howe, "Robotic catheter cardiac ablation combining ultrasound guidance and force control," *The International Journal of Robotics Research*, vol. 33, no. 4, pp. 631–644, 2014.

[19] L. Ott, F. Nageotte, P. Zanne, and M. De Mathelin, "Robotic assistance to flexible endoscopy by physiological-motion tracking," *IEEE Transactions on Robotics*, vol. 27, no. 2, pp. 346–359, 2011.

[20] P. M. Loschak, L. J. Brattain, and R. D. Howe, "Automated pointing of cardiac imaging catheters," in *IEEE International Conference on Robotics and Automation (ICRA)*, 2013, pp. 5794–5799.

[21] A. Degirmenci, P. M. Loschak, C. M. Tschabrunn, E. Anter, and R. D. Howe, "Compensation for unconstrained catheter shaft motion in cardiac catheters," in *2016 IEEE International Conference on Robotics and Automation (ICRA)*. IEEE, 2016, pp. 4436–4442.

[22] P. J. Parker and B. D. Anderson, "Frequency tracking of nonsinusoidal periodic signals in noise," *Signal Processing*, vol. 20, no. 2, pp. 127–152, 1990.

[23] P. M. Loschak, A. Degirmenci, Y. Tenzer, C. M. Tschabrunn, E. Anter, and R. D. Howe, "A four degree of freedom robot for positioning ultrasound imaging catheters," in *ASME J. Mechanisms Robotics*. American Society of Mechanical Engineers, 2016, pp. 051 016–051 016–9.